doi: 10.82124/CEAS-GNC-2026-027 CEAS-GNC-2026-027

EuroGNC Navigation Guidance Control CEAS Madrid, Spain May 5th-7th uc3m Universidad Carlos III de Madrid AIAA 2026

Trajectory Shaping Guidance for Field-of-View Constrained Impact Angle Control

Kun Wang Assistant Professor, Universidad Carlos III de Madrid, Department of Aerospace Engineering, 28911 Leganés, Spain. Corresponding author, kwang@ing.uc3m.es

ABSTRACT

In this paper we propose a trajectory shaping guidance law for directing a pursuer toward a stationary target with a prescribed impact angle, while satisfying a field-of-view (FOV) constraint. A saturated parameterization of the look angle based on the hyperbolic tangent function is employed, inherently enforcing the FOV constraint throughout the engagement. As a result, the guidance problem reduces to solving a univariate nonlinear equation for the guidance gain. Some properties of this smooth nonlinear equation are analyzed, enabling efficient and reliable solution via a bisection method with a first-order approximate initializer. Numerical simulations demonstrate the effectiveness of the proposed guidance law in achieving the desired impact angle while satisfying the FOV constraint.

Keywords: Nonlinear impact angle control, Field-of-view constraint, Trajectory shaping guidance, Hyperbolic tangent function

Nomenclature

(x, y)	=	position coordinates
γ	=	flight path angle
$\lambda, \lambda_{\mathrm{d}}$	=	LOS angle, desired LOS angle
$\sigma, \sigma_{\max}$	=	look angle, maximum permissible look angle
r	=	relative range
ρ	=	normalized relative range
V	=	pursuer's constant speed
a	=	acceleration
ψ, g, I, Δ	=	auxiliary variables
α	=	guidance gain
f	=	nonlinear equation for solving α
ε and ϵ	=	small positive constant
k, M	=	integer for bracketing expansion, number of samples for bracketing

1 Introduction

Impact angle control is a fundamental requirement in interception scenarios since it allows the pursuer to reach the target from a prescribed direction, thereby improving the observability and enhancing the

effectiveness of the strike [1–4]. Meanwhile, satisfying the field-of-view (FOV) constraint is essential to ensure that the target remains within the seeker's detection range throughout the engagement. To this end, there have been various efforts in the literature to design guidance laws that achieve impact angle control while satisfying the FOV constraint.

As the most popular guidance method, proportional navigation (PN) guidance has been widely extended to design the impact angle control guidance laws [1, 5, 6]. For instance, Kim *et al.* [1] embedded a time-varying bias term based on range-to-go into PN. Erer and Merttopcuoglu [5] developed a two-phase guidance strategy that switches from a biased PN to a conventional PN to achieve the desired impact angle. In addition, their guidance law does not require time-to-go nor range information. Linear optimal control theory has been employed to derive optimal guidance laws for impact angle control [7–10]. Specifically, by linearizing the kinematics around the collision triangle, optimal guidance laws under the effect of lag-free and first-order autopilots were obtained in Refs. [7, 8]. Chen and Wang [9] derived an optimal guidance law using the time-to-go estimation, and the strategy was also extended to control both the impact time and angle. Recently, to account for the aerodynamic drag in practical scenarios, Jung *et al.* [10] developed an optimal guidance law with two feedback terms.

The guidance performance of the methods in the aforementioned literature can be furthered improved by considering the nonlinear kinematics. Therefore, various nonlinear guidance laws have been proposed for impact angle control. The methods include but not limited to state-dependent Riccati equation [11], sliding mode control [12], trajectory shaping [2], to name a few. For instance, Kumar and Maity in Ref. [11] converted the impact angle control guidance problem to a tracking problem by leveraging the relationship between the impact angle and line-of-sight (LOS) angle. Ref. [12] employed sliding mode control to enforce the impact angle to reach the desired value in finite time. In addition, the proposed method in Ref. [12] is applicable to intercepting constant velocity and maneuvering targets. On the other hand, trajectory shaping guidance involves representing the geometric shape of the state or the guidance command with mathematical expressions. By embedding the boundary conditions, the impact angle guidance problem can be reduced to solving some nonlinear equations.

It is worth noting that these guidance laws do not explicitly account for the control effort, which may result in excessive energy consumption. To address this issue, nonlinear optimal guidance laws have attracted increasing attention in recent years. Deriving a nonlinear optimal guidance law is essentially equivalent to solving the corresponding nonlinear optimal control problem in real time, which is generally challenging due to the requirement for appropriate initial guesses or the high computational burden involved [13, 14]. To overcome these difficulties, machine learning techniques have been increasingly employed to approximate the nonlinear optimal control [3, 15–17]. For instance, the parameterization of the optimal trajectory proposed in Ref. [15] was extended to a nonlinear optimal impact control problem in Ref. [16]. To address the issue that the final acceleration is typically nonzero, Ref. [3] introduced a regularization method for the final acceleration. However, these studies do not take into account the FOV constraint. From a practical standpoint, the FOV constraint should be incorporated to ensure that the target remains within the seeker's detection range throughout the engagement, particularly in impact angle control scenarios with curved flight trajectory.

To satisfy the FOV constraint, various methods have been proposed in the literature. For instance, Fu *et al.* [2] introduced a third-order polynomial with respect to the LOS angle. By analyzing the relationship between the look angle and the guidance coefficient, the authors derived the boundary of the coefficient that satisfies the FOV constraint. In Ref. [18], a range-to-go weighted optimal control problem was solved, where the FOV constraint was treated as a state inequality constraint. Hu *et al.* [19] proposed a cubic polynomial to parameterize the look angle profile, expressing the FOV constraint as functions of the polynomial coefficients. Additionally, Ref. [20] employed a reinforcement learning approach to train an agent to learn bias terms, addressing impact-angle and FOV constraints separately. In Ref. [21], a sufficient condition for satisfying the FOV constraint under a relative virtual reference frame was derived.

Tekin and Erer [22] designed a switched guidance law, where the look angle and acceleration constraints were enforced by numerically solving for the required midcourse and terminal navigation gains. More recently, Ref. [23] utilized a nonlinear function to ensure that the look angle remains within the FOV constraint.

In summary, to satisfy the FOV constraint, most existing methods rely on either a switched strategy or the tuning of additional parameters. Such approaches increase the complexity of the guidance law and may result in nonsmooth or even discontinuous guidance commands. To the best of the authors' knowledge, a nonlinear guidance law that achieves impact angle control while inherently satisfying the FOV constraint, without relying on a switched strategy or tuning any design parameters, is rarely seen in the literature. To address this, we extend the method in Ref. [24] to the FOV-constrained impact angle control problem. The main contributions are summarized as follows:

(1) A saturated parameterization of the look angle based on the hyperbolic tangent function is employed, inherently enforcing the FOV constraint throughout the engagement.
(2) The guidance problem is reduced to solving a univariate nonlinear equation for the guidance gain. Some properties of this nonlinear equation are analyzed, enabling efficient and reliable solution via a bisection method with a first-order approximate initializer.
(3) The proposed guidance law is not only continuous but also smooth, and it does not require tuning of the design parameters, making it easy to implement in practice.

The remainder of this paper is organized as follows. Section 2 presents the problem formulation. Section 3 details the design of the proposed guidance law, followed by numerical simulations in Section 4. Finally, conclusions are drawn in Section 5.

2 Problem Formulation

We consider the guidance geometry illustrated in Fig. 1. The origin of the Cartesian inertial reference frame Oxy is located at the target, denoted by T. Denote by $(x, y) \in \mathbb{R}^2$ the pursuer's position (denoted by P). The flight path angle $\gamma \in [-\pi, \pi]$ is defined to be the angle between the x axis and the pursuer's velocity $\boldsymbol{V}$. The angle between the LOS and the velocity $\boldsymbol{V}$ is called look angle $\sigma \in [-\pi, \pi]$. The angle between the LOS and the x axis is $\lambda \in [-\pi, \pi]$. The angles γ, σ, and λ are considered positive when measured counterclockwise from the designated reference axis. In addition, the relative range between the pursuer and target is denoted by r. Let $a \in \mathbb{R}$ represent the normal acceleration. The pursuer's velocity $\boldsymbol{V}$ has a magnitude of $V \in \mathbb{R}_+$. By normalizing V to unity, the pursuer's nonlinear kinematics can be described by [22]

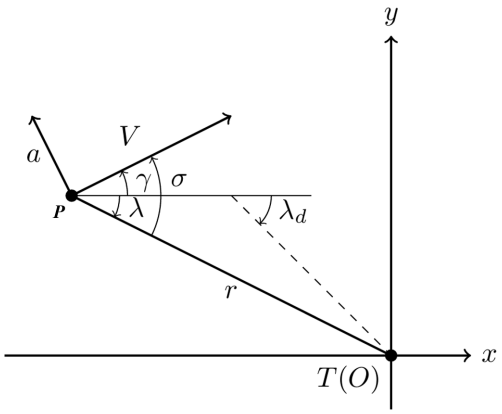

Fig. 1 Two-dimensional guidance geometry.

$$\begin{cases} \dot{r}(t) &= -\cos\sigma(t), \\ \dot{\lambda}(t) &= -\sin\sigma(t)/r(t), \\ \dot{\gamma}(t) &= a(t), \end{cases} \tag{1}$$

In addition, we have the following geometric relationship:

$$\sigma(t) = \gamma(t) - \lambda(t). \tag{2}$$

The initial conditions of the pursuer are

$$r(0) = r_0 > 0, \quad \lambda(0) = \lambda_0, \quad \gamma(0) = \gamma_0. \tag{3}$$

To reach the target at a desired angle λ_d with finite acceleration ensured by $\sigma(t_f) = 0$, the final conditions are specified by

$$r(t_f) = 0, \quad \lambda(t_f) = \gamma(t_f) = \lambda_\mathrm{d}, \tag{4}$$

where the final time t_f is free.

Under the assumption of small angles of attack, the lead angle defined in the velocity vector becomes identical to the look angle defined in the body axis [18]. That is, to ensure that the target remains within the seeker's FOV, we enforce an equivalent constraint on the look angle as follows:

$$|\sigma(t)| \le \sigma_\mathrm{max} \quad \text{for all } t \in [0, t_f] \quad \text{and} \qquad 0 < \sigma_\mathrm{max} < \frac{\pi}{2}. \tag{5}$$

3 Guidance Law Design

In this section, we present the design of the proposed guidance law. The main idea is to parameterize the look angle $\sigma(t)$ in a manner that inherently satisfies the FOV constraint in Eq. (5) and the final condition $\sigma(t_f) = 0$. This parameterization transforms the guidance problem into solving a univariate nonlinear equation for the guidance gain. Then, we analyze some properties of this smooth nonlinear equation, which enables efficient and reliable solution via a bisection method with a first-order approximate initializer.

3.1 Parameterization of the look angle

Let us define the normalized range $\rho := r/r_0 \in [0, 1]$. With Eq. (1), we obtain

$$\dot{\rho} = -\frac{\cos\sigma}{r_0}, \tag{6}$$

which further leads to

$$\frac{d\lambda}{d\rho} = \frac{\dot{\lambda}}{\dot{\rho}} = \frac{\tan\sigma}{\rho}. \tag{7}$$

In addition, the normal acceleration can be expressed as

$$a = \dot{\gamma} = \dot{\lambda} + \dot{\sigma} = -\frac{1}{r_0}\left(\cos\sigma\,\frac{d\sigma}{d\rho} + \frac{\sin\sigma}{\rho}\right). \tag{8}$$

Integrating Eq. (7) from $\rho = 1$ to $\rho = 0$ and applying the initial and final conditions in Eqs. (3) and (4) yields

$$\lambda_{\mathrm{d}} - \lambda_0 \;=\; -\int_0^1 \frac{\tan\sigma(\rho)}{\rho}\, d\rho \;. \tag{9}$$

To enforce the constraint in Eq. (5), we parameterize σ through a bounded hyperbolic tangent function as

$$\sigma(\rho) \;=\; \sigma_{\max}\, \tanh\big(\psi(\rho)\big), \tag{10}$$

where $\psi(\rho)$ is an affine function of ρ

$$\psi(\rho) = \psi_0\rho + \alpha\rho(1-\rho). \tag{11}$$

The parameters ψ_0 and α are to be determined. Equation (10) guarantees that the FOV constraint $|\sigma(\rho)| \le \sigma_{\max}$ holds.

With Eq. (11), it is observed that $\sigma(\rho)$ vanishes as $\rho \to 0$. Therefore, the integral in Eq. (9) remains finite. At impact, i.e., $\rho = 0$, it is obvious that the constraint $\sigma(0) = 0$ is enforced by $\psi(0) = 0$. Considering the initial time, i.e., $\rho = 1$, $\sigma(1) = \sigma_0 = \sigma_{\max}\tanh(\psi_0)$, we obtain

$$\psi_0 = \operatorname{arctanh}\!\left(\frac{\sigma_0}{\sigma_{\max}}\right). \tag{12}$$

Hence the parameterized look angle in Eq. (10) is solely determined by the guidance gain α. Notice that, to ensure numerical stability, a saturation operator is applied to the argument of the arctanh function when σ_0 approaches $\pm\sigma_{\max}$. Specifically, we define

$$\psi_0 = \operatorname{arctanh}\!\left(\mathrm{sat}\!\left(\frac{\sigma_0}{\sigma_{\max}}\right)\right), \tag{13}$$

where the saturation operator is given by

$$\mathrm{sat}(x) = \max\big(\min(x,\, 1-\epsilon),\, -1+\epsilon\big), \tag{14}$$

with a small constant $\epsilon > 0$ (e.g., $\epsilon = 10^{-9}$) to avoid the singularity of the arctanh$(\cdot)$ function at ± 1.

Substituting Eq. (10) into Eq. (9) gives a nonlinear equation in terms of α, i.e.,

$$f(\alpha) := \underbrace{\int_0^1 \frac{\tan\big(\sigma_{\max}\tanh(\psi_0\rho + \alpha\rho(1-\rho))\big)}{\rho}\, d\rho}_{=:I(\alpha)} - \underbrace{(\lambda_0 - \lambda_{\mathrm{d}})}_{=:\Delta} = 0, \tag{15}$$

It is obvious that $\Delta \in [-2\pi, 2\pi]$. Up to this point, the guidance problem is reduced to solving the nonlinear equation Eq. (15) for the guidance gain α.

3.2 Some properties of the function $I(\alpha)$

3.2.1 Monotonicity and Existence of the Solution

Considering $\rho \to 0$, we have

$$\psi(\rho) \sim (\psi_0 + \alpha)\rho, \qquad \sigma(\rho) \sim \sigma_{\max}(\psi_0 + \alpha)\rho, \qquad \frac{\tan\sigma(\rho)}{\rho} \sim \sigma_{\max}(\psi_0 + \alpha). \tag{16}$$

With Eq. (15), the derivative of $f(\alpha)$ can be obtained as

$$f'(\alpha) = I'(\alpha) = \int_0^1 \sec^2\big(\sigma(\rho)\big)\, \frac{\partial \sigma}{\partial \alpha}(\rho)\, \frac{d\rho}{\rho}. \tag{17}$$

From the definition of $\sigma(\rho)$ in (10), one has $\partial\sigma/\partial\alpha = \sigma_{\max} \operatorname{sech}^2\big(\psi(\rho)\big)\rho(1-\rho)$. Substituting this expression into (17) yields

$$I'(\alpha) = \int_0^1 \sigma_{\max} \sec^2\big(\sigma(\rho)\big) \operatorname{sech}^2\big(\psi(\rho)\big)(1-\rho)\, d\rho. \tag{18}$$

For any $\rho \in (0,1)$, the integrand in (18) is strictly positive, as it is composed of the product of positive terms: $\sigma_{\max} > 0$, $\sec^2\sigma \geq 1$, $\operatorname{sech}^2\psi > 0$, and $(1-\rho) > 0$. Note that as $\rho \to 0$, both $\sec^2\sigma$ and $\operatorname{sech}^2\psi$ approach unity, which ensures that the integrand is well-defined and positive in the neighborhood of the origin. Since the integrand is continuous and strictly positive on $(0,1)$, the integral $I'(\alpha)$ is positive for any $\alpha \in \mathbb{R}$. Therefore, the function $I(\alpha)$ is *strictly increasing*.

Additionally, because the linear term dominates for small ρ, we have

$$I(\alpha) = \varepsilon\sigma_{\max}(\psi_0 + \alpha) + O(1) \quad \Rightarrow \quad \lim_{\alpha\to\pm\infty} f(\alpha) = \pm\infty. \tag{19}$$

Therefore, it can be concluded that the function $I(\alpha)$ is strictly increasing with limits $\lim_{\alpha\to\pm\infty} f(\alpha) = \pm\infty$. Hence Eq. (15) *admits a unique root* for any $\Delta \in [-2\pi, 2\pi]$.

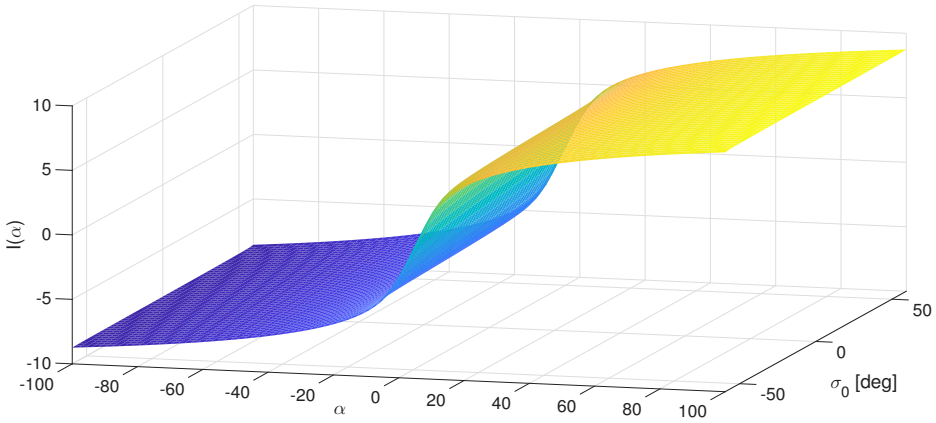

Fig. 2 Function $I(\alpha)$ for $\sigma_{\max} = 60$ deg with $\alpha \in [-100, 100]$ and $\sigma_0 \in (-\sigma_{\max}, \sigma_{\max})$.

3.2.2 Oddness of the Function $I(\alpha)$ for $\sigma_0 = 0$

In the special case of $\sigma_0 = 0$ (i.e., $\psi_0 = 0$), we show that $I(\alpha)$ is an odd function of α. This property is useful for constructing a bracketing interval for the root-finding algorithm.

Consider the function

$$I(\alpha) = \int_0^1 g(\rho,\alpha)\, d\rho, \qquad \text{with} \qquad g(\rho,\alpha) := \frac{\tan\big(\sigma_{\max}\tanh(\alpha\,\rho(1-\rho))\big)}{\rho}.$$

For fixed $\rho \in (0,1]$, define $u(\rho,\alpha) := \alpha\rho(1-\rho)$. Since both $\tanh(\cdot)$ and $\tan(\cdot)$ are odd functions, we have

$$g(\rho,-\alpha) = \frac{\tan\big(\sigma_{\max}\tanh(-u(\rho,\alpha))\big)}{\rho} = -\frac{\tan\big(\sigma_{\max}\tanh(u(\rho,\alpha))\big)}{\rho} = -g(\rho,\alpha). \tag{20}$$

Thus the integrand is odd in α for every fixed $\rho > 0$. It is clear that $g(\rho, \alpha)$ remains finite as $\rho \to 0^+$. Thus $g(\cdot, \alpha)$ is continuous and integrable on $[0, 1]$.

Since $g(\rho, -\alpha) = -g(\rho, \alpha)$ for all $\rho \in [0, 1]$ and $g(\cdot, \alpha)$ is integrable, we can interchange sign and integration, i.e.,

$$I(-\alpha) = \int_0^1 g(\rho, -\alpha)\, d\rho = -\int_0^1 g(\rho, \alpha)\, d\rho = -I(\alpha), \tag{21}$$

completing the proof.

3.3 Solving the guidance gain

In this subsection, we present a robust numerical procedure to solve Eq. (15) for the guidance gain α. To obtain an initializer for α, substituting the third approximation in Eq. (16) into the integral yields

$$\int_0^1 \frac{\tan(\sigma_{\max} \tanh(\psi(\rho; \alpha)))}{\rho}\, d\rho \approx \int_0^1 \sigma_{\max}(\psi_0 + \alpha)\, d\rho = \sigma_{\max}(\psi_0 + \alpha). \tag{22}$$

Imposing the boundary condition $f(\alpha_0) \approx 0$ gives the first-order analytic initializer

$$\alpha_0 = \frac{\Delta}{\sigma_{\max}} - \psi_0. \tag{23}$$

To ensure robust convergence of the root-finding algorithm, a bracketing interval $[\alpha_L, \alpha_R]$ is constructed around α_0. Starting from α_0, expand the bracket geometrically: $\alpha_L \leftarrow \alpha_L - 2^k$, $\alpha_R \leftarrow \alpha_R + 2^k$ ($k = 0, 1, 2, \ldots$) until $f(\alpha_L) f(\alpha_R) \le 0$. For each expansion, M equally spaced samples $\alpha_i \in [\alpha_0 - 2^k, \alpha_0 + 2^k]$ are evaluated. If a sign change between consecutive samples is detected, the corresponding pair $[\alpha_L, \alpha_R]$ is taken as a valid bracket containing the root. This procedure is guaranteed to succeed because $f(\alpha)$ is monotonic and diverges as $\alpha \to \pm\infty$. Once a valid bracket is obtained, the unique root α is computed using MATLAB's *fzero* function applied to $[\alpha_L, \alpha_R]$.

It is worth noting that, in the special case of $\sigma_0 = 0$, the function $I(\alpha)$ is an odd function. This property permits the use of a symmetric bracketing interval centered at the initial estimate α_0, thereby improving the efficiency and numerical stability of the root-finding procedure. Without loss of generality, let $\Delta > 0$; then, the initial value given by Eq. (23) reduces to $\alpha_0 = \Delta/\sigma_{\max} > 0$. Consequently, the corresponding root α must also be positive, as illustrated by Fig. 2.

4 Numerical Simulations

To validate the effectiveness of the proposed guidance law, numerical simulations are conducted in this section. First, the performance of the proposed guidance law is evaluated for different desired impact angles, initial look angles, and maximum permissible look angles. Then, a comparison with other existing guidance laws is presented. In the procedure for solving the guidance gain α, the integer for bracketing expansion and the number of samples for bracketing are set as $k = 7$ and $M = 100$, respectively.

4.1 Different impact angles

The pursuer's initial conditions are set as $r_0 = 3$ km, $\lambda_0 = -90$ deg, and $\gamma_0 = -90$ deg. The desired impact angles are $\lambda_d = 0$ and -180 deg, and the maximum permissible look angle is $\sigma_{\max} = 60$ deg. The pursuer's speed is 200 m/s. It is obvious that the initial look angle is $\sigma_0 = 0$ deg and the impact angle errors are $\Delta = \mp 90$ deg.

The guidance gain α is computed to be -2.9953 and 2.9953 for the two desired impact angles, respectively. Figures 3, 4, and 5 illustrate the flight trajectories, look angle profiles, and guidance command profiles for the two desired impact angles. It is observed that the pursuer successfully achieves the desired impact angles while satisfying the FOV constraint throughout the engagement. The acceleration profiles demonstrate smooth transitions. The results confirm the symmetric nature of the trajectories and guidance commands for opposite impact angle errors in the case of $\sigma_0 = 0$.

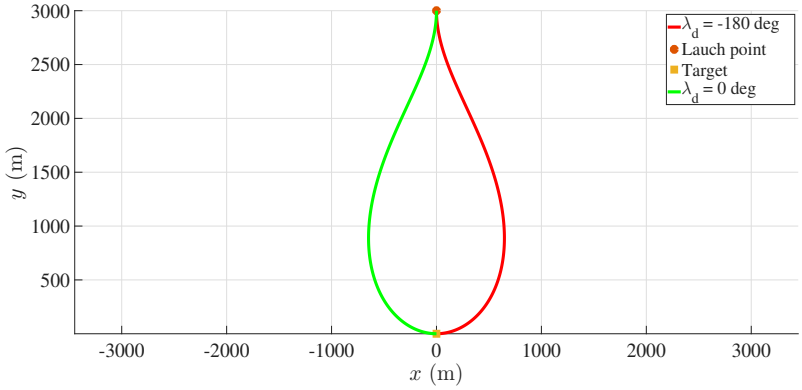

Fig. 3 Flight trajectories for different impact angles.

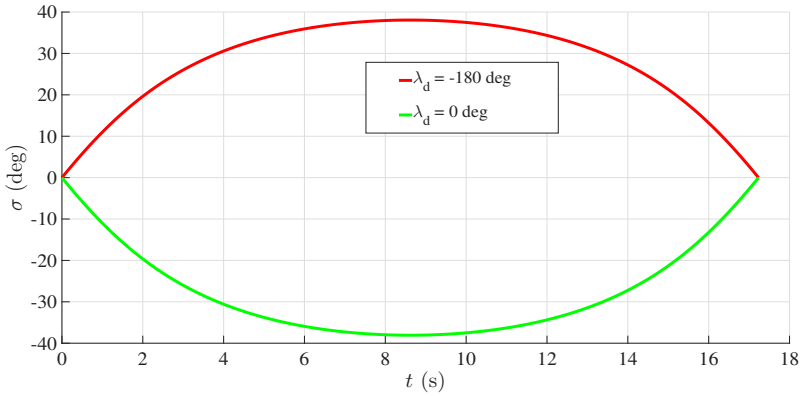

Fig. 4 Look angle profiles for different impact angles.

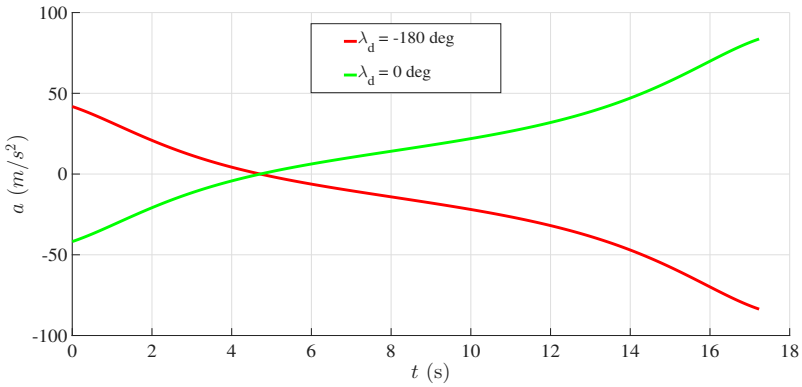

Fig. 5 Guidance command profiles for different impact angles.

4.2 Different initial look angles

The pursuer's initial conditions are set as $r_0 = 3$ km, $\lambda_0 = 180$ deg. The desired impact angle is $\lambda_d = 0$ deg, and the maximum permissible look angle is $\sigma_{max} = 90$ deg. The pursuer's speed is 300 m/s. The initial look angles are set as $\sigma_0 = -10, -20, -60$, and -80 deg. Figure 6 illustrates the flight trajectories for the different initial look angles. The look angle profiles in Fig. 7 confirm that the FOV constraint is satisfied throughout the engagement. The guidance command profiles in Fig. 8 demonstrate smooth transitions. These results validate the effectiveness of the proposed guidance law in achieving the desired impact angle while adhering to the FOV constraint for various initial look angles.

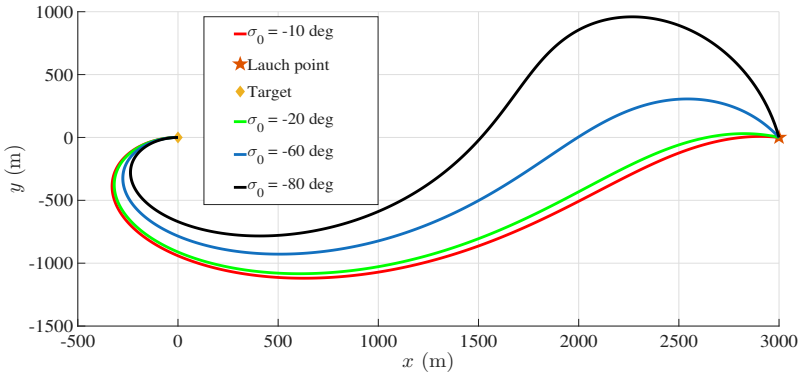

Fig. 6 Flight trajectories for various initial look angles.

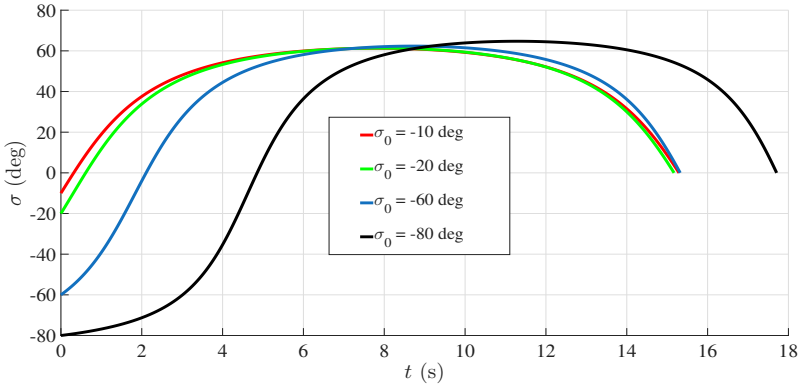

Fig. 7 Look angle profiles for various initial look angles.

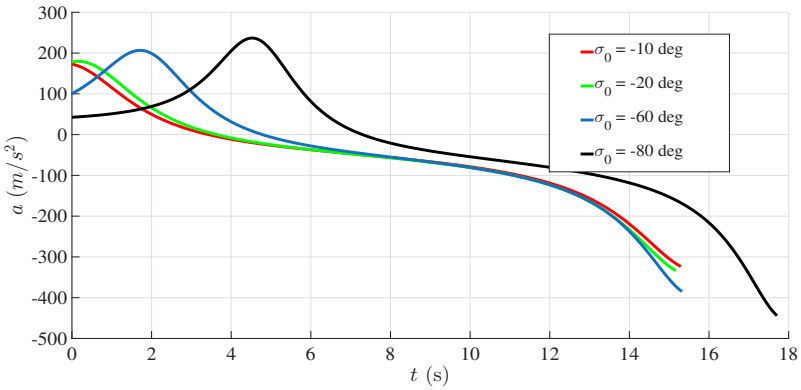

Fig. 8 Guidance command profiles for various initial look angles.

4.3 Different maximum permissible look angles

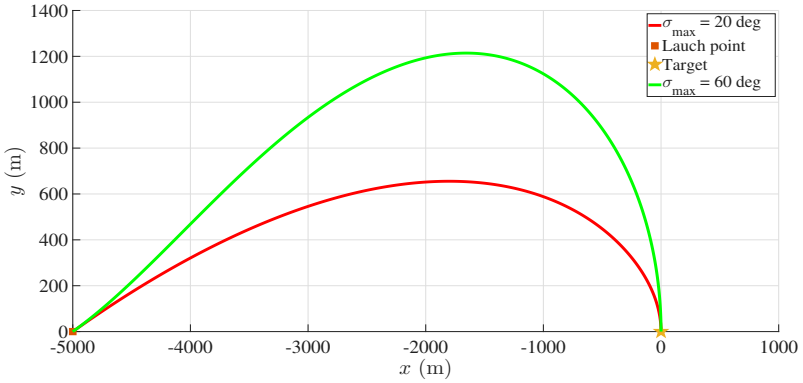

Fig. 9 Flight trajectories for different maximum permissible look angles.

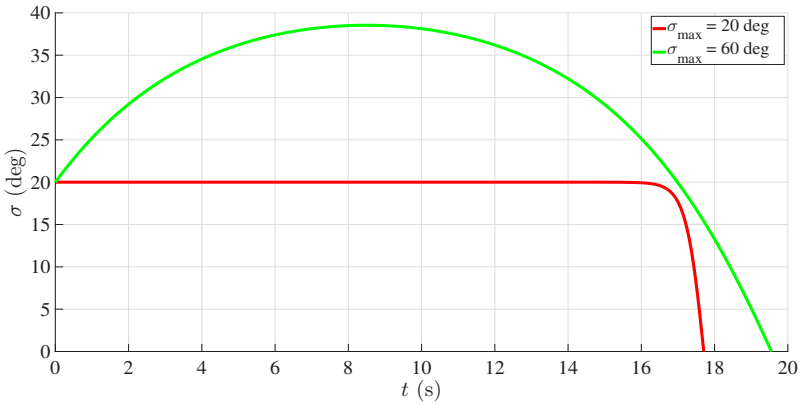

Fig. 10 Look angle profiles for different maximum permissible look angles.

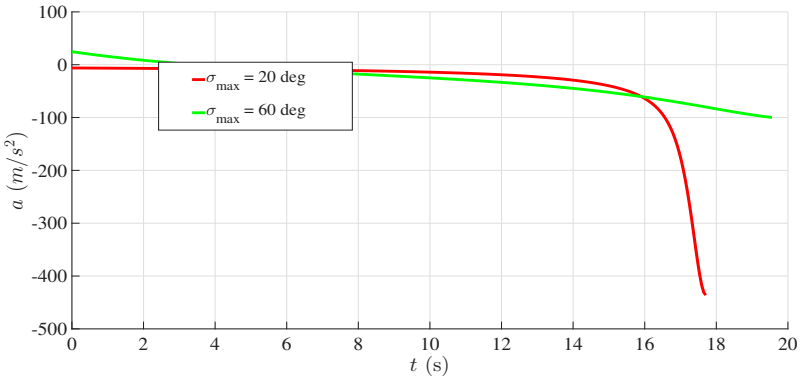

Fig. 11 Guidance command profiles for different maximum permissible look angles.

The pursuer's initial conditions are set as $r_0 = 5$ km, $\lambda_0 = 0$ deg, and $\gamma_0 = 20$ deg. The desired impact angle is $\lambda_d = -90$ deg, and the maximum permissible look angles are $\sigma_{max} = 20$ and 60 deg. The pursuer's speed is 300 m/s. The flight trajectories for the different maximum permissible look angles are illustrated in Fig. 9. As the maximum permissible look angle increases, the pursuer's trajectory becomes less curved, leading to a longer time of flight, as confirmed by Fig. 10. From Fig. 10, it is observed that the look angle profiles remain within the specified FOV constraints throughout the engagement. In addition, the guidance command profiles in Fig. 11 demonstrate smooth transitions for both maximum

Table 2 Guidance gains and the extremum of the look angle for different $\sigma_{\max}$

Item	Guidance gain	Extremal look angle (deg)
$\sigma_{\max} = 20$ deg	24	20.00
$\sigma_{\max} = 60$ deg	2.30	38.54

permissible look angles. The guidance gains and the extremum of the look angle for the different maximum permissible look angles are summarized in Table 2. It is observed that as the maximum permissible look angle increases, the guidance gain decreases. In addition, the extremum of the look angle is less likely to reach the maximum permissible look angle.

4.4 Comparative study

We consider a comparative study between the proposed guidance law and two existing methods: the two-stage PN-based guidance law by Ratnoo [6] and the time-to-go inversion guidance by Li *et al.* [23]. To be more specific, the guidance gain is set to $N = 1$ and $N = 2$ for the first and second stages of Ratnoo's law, respectively. In addition, the parameter η to control the starting point of the FOV constraint in Li's law is set to 0.8. To cases are considered.

Case A. The pursuer's initial conditions are set as $r_0 = 10$ km, $\lambda_0 = 0$ deg, and $\sigma_0 = 45$ deg. The desired impact angle is $\lambda_d = -90$ deg, and the maximum permissible look angle is $\sigma_{\max} = 50$ deg. The pursuer's speed is 300 m/s. Figures 12, 13, and 14 illustrate the flight trajectories, look angle profiles, and guidance command profiles obtained using different guidance laws. All three guidance laws successfully achieve the desired impact angle while satisfying the FOV constraint throughout the engagement. The proposed law yields the smoothest acceleration profile. For better illustration, Table 3 summarizes the key performance metrics of each guidance law. The control effort is computed as $J = \int_0^{t_f} a^2(t)\, dt$. It is observed that only the proposed guidance law yields a smooth acceleration profile. In addition, the control effort of the proposed guidance law is significantly smaller than that of Li's law.

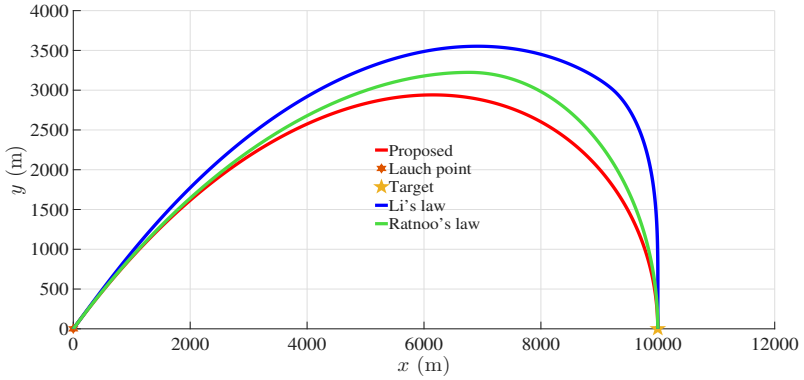

Fig. 12 Flight trajectories obtained by different guidance laws.

Table 3 Comparison of the guidance performance using different guidance laws

Guidance Law	J (m^2/s^3)	Extremal Acceleration (m/s^2)	Extremal Look Angle (deg)	Smooth
Proposed Law	1.58×10^4	−39.13	45	Yes
Ratnoo's Law	1.54×10^4	−27.92	45	No
Li's Law	2.13×10^4	−76.80	49.08	No

Case B. The initial conditions are set as $r_0 = 8$ km, $\lambda_0 = 0$ deg, and $\sigma_0 = 0$ deg. The desired impact angle is $\lambda_d = -120$ deg, and the maximum permissible look angle is $\sigma_{\max} = 60$ deg. The pursuer's speed

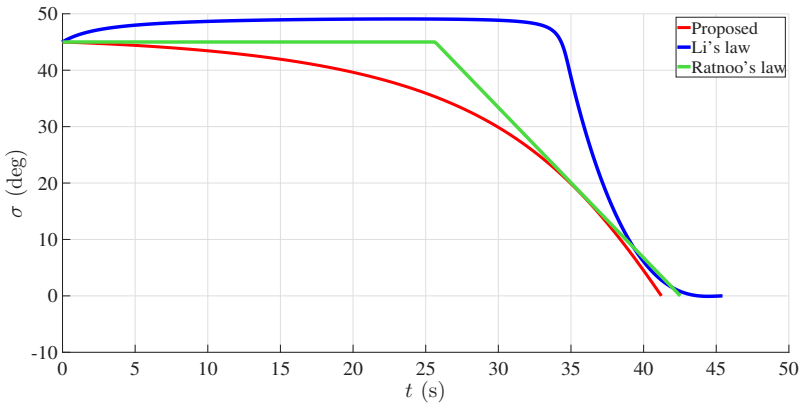

Fig. 13 Look angle profiles obtained by different guidance laws.

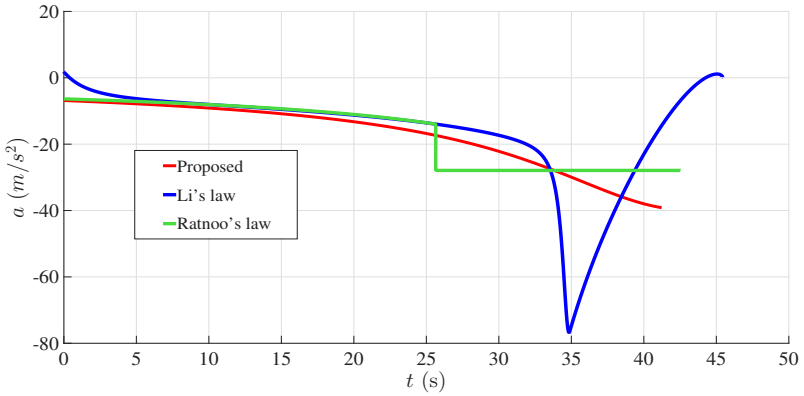

Fig. 14 Guidance command profiles obtained by different guidance laws.

is 300 m/s. The flight trajectories, look angle profiles, guidance commands, and control effort profiles obtained using different guidance laws are illustrated in Fig. 15. It is observed that only the proposed method and Li's law successfully achieve the desired impact angle while satisfying the FOV constraint throughout the engagement. The reason for the failure of Ratnoo's law is that it requires the pursuer to be launched with a deviated look angle, making it inapplicable when the initial heading angle error is zero. In addition, the proposed law yields a smoother acceleration profile than Li's law, as shown by Fig. 15c. The control effort of the proposed guidance law is also smaller than that of Li's law, as shown by Fig. 15d.

5 Conclusions

In this paper a trajectory shaping guidance law was proposed to achieve impact angle control while satisfying the FOV constraint. The look angle was parameterized using a bounded hyperbolic tangent function, inherently enforcing the FOV constraint throughout the engagement. The guidance problem was reduced to solving a univariate nonlinear equation for the guidance gain. Some properties of this nonlinear equation were analyzed, enabling efficient and reliable solution via a bisection method with a first-order approximate initializer. Numerical simulations validated the effectiveness of the proposed guidance law in achieving the desired impact angle while adhering to the FOV constraint for various initial conditions. In addition, the guidance command profile is smooth and there is no need to tune any design parameters, making it easy for practical implementation. Future work may include extending the proposed guidance law to three-dimensional scenarios.

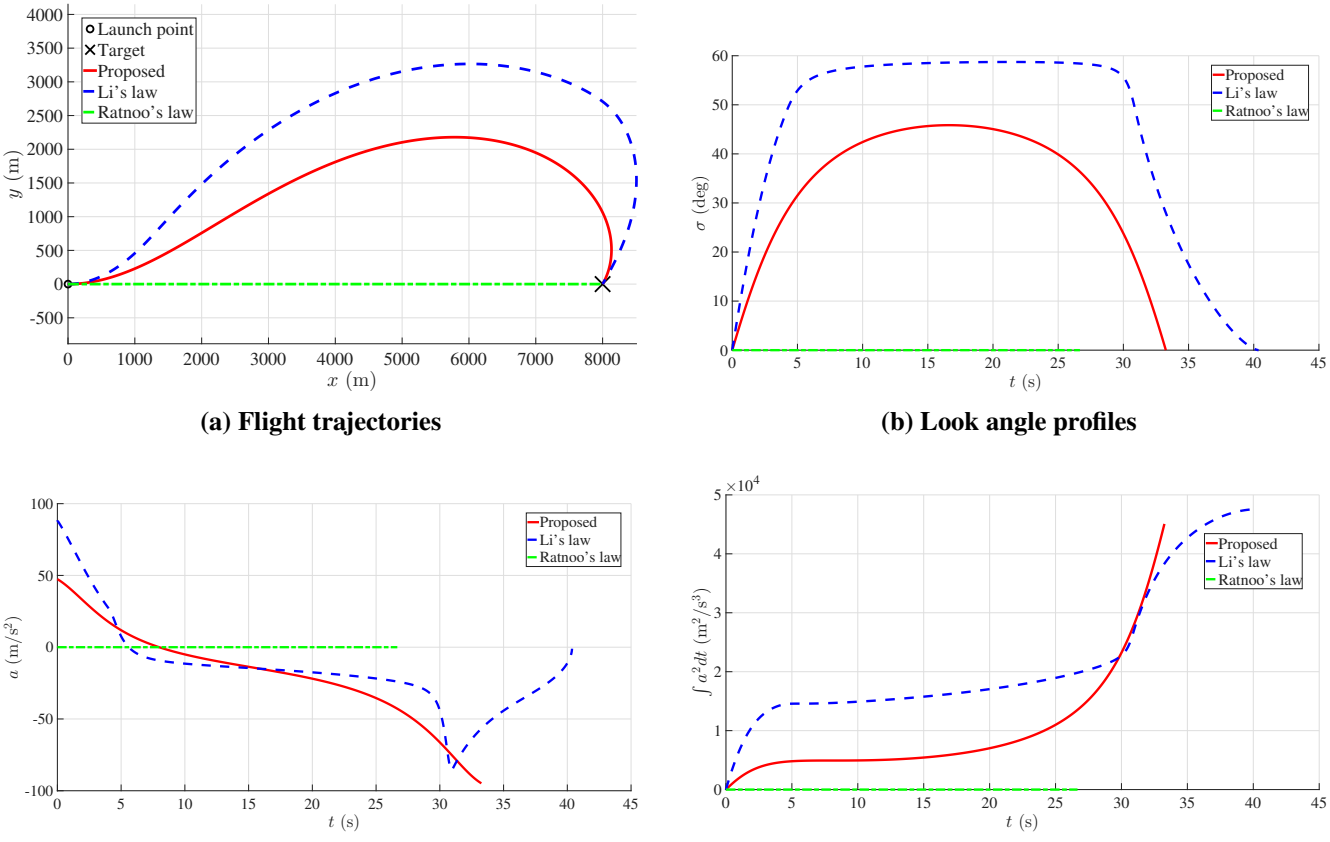

(a) Flight trajectories

(b) Look angle profiles

(c) Acceleration profiles

(d) Control effort profiles

Fig. 15 Case B: Simulation comparison of the Proposed method, Li's law, and Ratnoo's law.

Acknowledgments

The author acknowledges the support by the grants for research activity of young PhD holders, part of the Universidad Carlos III de Madrid (UC3M) Own Research Program (Ayudas para la Actividad Investigadora de los Jóvenes Doctores, del Programa Propio de Investigación de la UC3M).

Declaration of Use of Artificial Intelligence

Artificial intelligence was used for proofreading the manuscript.

References

[1] Byung Soo Kim, Jang Gyu Lee, and Hyung Seok Han. Biased PNG law for impact with angular constraint. *IEEE Transactions on Aerospace and Electronic Systems*, 34(1):277–288, 1998. doi: 10.1109/7.640285.

[2] Shengnan Fu, Guanqun Zhou, and Qunli Xia. A trajectory shaping guidance law with field-of-view angle constraint and terminal limits. *Journal of Systems Engineering and Electronics*, 33(2):426–437, 2022. doi: 10.23919/JSEE.2022.000043.

[3] Kun Wang, Fangmin Lu, and Zheng Chen. Nonlinear optimal impact angle control guidance with acceleration constraints. *IEEE Transactions on Aerospace and Electronic Systems*, 61(4):8907–8921, 2025. doi: 10.1109/TAES.2025.3551283.

[4] Yuan Zheng, Zheng Chen, Xueming Shao, and Wenjie Zhao. Time-optimal guidance for intercepting moving targets with impact-angle constraints. *Chinese Journal of Aeronautics*, 35(7):157–167, 2022. doi: 10.1016/j.cja.2021.08.002.

[5] Koray S Erer and Osman Merttopçuoglu. Indirect impact-angle-control against stationary targets using biased pure proportional navigation. *Journal of Guidance, Control, and Dynamics*, 35(2):700–704, 2012. doi: 10.2514/1.52105.

[6] Ashwini Ratnoo. Analysis of two-stage proportional navigation with heading constraints. *Journal of Guidance, Control, and Dynamics*, 39(1):156–164, 2016. doi: 10.2514/1.G001262.

[7] Chang-Kyung Ryoo, Hangju Cho, and Min-Jea Tahk. Optimal guidance laws with terminal impact angle constraint. *Journal of Guidance, Control, and Dynamics*, 28(4):724–732, 2005. doi: 10.2514/1.8392.

[8] Chang-Kyung Ryoo, Hangju Cho, and Min-Jea Tahk. Time-to-go weighted optimal guidance with impact angle constraints. *IEEE Transactions on Control Systems Technology*, 14(3):483–492, 2006. doi: 10.1109/TCST.2006.872525.

[9] Xiaotian Chen and Jinzhi Wang. Optimal control based guidance law to control both impact time and impact angle. *Aerospace Science and Technology*, 84:454–463, 2019. doi: 10.1016/j.ast.2018.10.036.

[10] Cheol-Goo Jung and Chang-Hun Lee. Optimal impact angle control guidance law considering aerodynamic drag. *Journal of Guidance, Control, and Dynamics*, 47(11):2435–2443, 2024. doi: 10.2514/1.G008234.

[11] Shashi Ranjan Kumar and Arnab Maity. Finite-horizon robust suboptimal control-based impact angle guidance. *IEEE Transactions on Aerospace and Electronic Systems*, 56(3):1955–1965, 2019. doi: 10.1109/TAES.2019.2938126.

[12] Shashi Ranjan Kumar, Sachit Rao, and Debasish Ghose. Nonsingular terminal sliding mode guidance with impact angle constraints. *Journal of Guidance, Control, and Dynamics*, 37(4):1114–1130, 2014. doi: 10.2514/1.62737.

[13] Kun Wang, Fangmin Lu, Zheng Chen, and Jun Li. A physics-informed indirect method for trajectory optimization. *IEEE Transactions on Aerospace Electronic Systems*, 60(6):9179–9192, 2024. doi: 10.1109/TAES.2024.3438687.

[14] Kun Wang, Zheng Chen, Zhenyu Wei, Fangmin Lu, and Jun Li. A new smoothing technique for bang-bang optimal control problems. In *AIAA SCITECH 2024 Forum*, page 0727, 2024. doi: 10.2514/6.2024-0727.

[15] Kun Wang, Zheng Chen, Han Wang, Jun Li, and Xueming Shao. Nonlinear optimal guidance for intercepting stationary targets with impact-time constraints. *Journal of Guidance, Control, and Dynamics*, 45(9):1614–1626, 2022. doi: 10.2514/1.G006666.

[16] Lin Cheng, Han Wang, Shengping Gong, and Xu Huang. Neural-network-based nonlinear optimal terminal guidance with impact angle constraints. *IEEE Transactions on Aerospace and Electronic Systems*, 60(1):819–830, 2023. doi: 10.1109/TAES.2023.3328576.

[17] Fanchen Wu, Zheng Chen, Xueming Shao, and Kun Wang. Nonlinear optimal guidance with constraints on impact time and impact angle. *Automatica*, 181:112500, 2025. doi: 10.1016/j.automatica.2025.112500.

[18] Bong-Gyun Park, Tae-Hun Kim, and Min-Jea Tahk. Range-to-go weighted optimal guidance with impact angle constraint and seeker's look angle limits. *IEEE Transactions on Aerospace and Electronic Systems*, 52(3):1241–1256, 2016. doi: 10.1109/TAES.2016.150415.

[19] Qinglei Hu, Ruihao Cao, Tuo Han, and Ming Xin. Field-of-view limited guidance with impact angle constraint and feasibility analysis. *Aerospace Science and Technology*, 114:106753, 2021. doi: 10.1016/j.ast.2021.106753.

[20] Sangmin Lee, Youngjun Lee, Youdan Kim, Yongsu Han, Hyuckhoon Kwon, and Daseon Hong. Impact angle control guidance considering seeker's field-of-view limit based on reinforcement learning. *Journal of Guidance, Control, and Dynamics*, 46(11):2168–2182, 2023. doi: 10.2514/1.G007715.

[21] Pengyu Wang, Honglong Kang, and Chang-Hun Lee. Field-of-view limited guidance law for maneuvering targets using relative virtual frame formulation. In *The 7th CEAS Conference on Guidance, Navigation and Control, EuroGNC 2024*. Council of European Aerospace Societies (CEAS), 2024. doi: 10.82124/CEAS-GNC-2024-036.

[22] Raziye Tekin and Koray S Erer. Switched-gain guidance for impact angle control under physical constraints. *Journal of Guidance, Control, and Dynamics*, 38(2):205–216, 2015. doi: 10.2514/1.G000766.

[23] Qiuya Li, Xinglong Li, Pengyu Wang, and Yanning Guo. Time-to-go inversion guidance considering impact and field-of-view constraints. In *2025 44th Chinese Control Conference (CCC)*, pages 4299–4304, 2025. doi: 10.23919/CCC64809.2025.11179485.

[24] Kun Wang, Zhenyu Wei, and Pengyu Wang. Look-angle-shaped impact time control guidance with field-of-view constraints. *Aerospace Science and Technology*, 176:112131, 2026. doi: 10.1016/j.ast.2026.112131.